Third International Conference on CFD in the Minerals and Process Industries
CSIRO, Melbourne, Australia
10-12 December 2003

MODELLING OF AIR FLOW AND POLLEN COLLECTION BY A SINGLE KIWIFRUIT FLOWER UNDER WIND AND AN AIR JET

Michael J.W. Hll, John ABRAHAMSON and Patrick J. JORDAN

Chemical and Process Engineering, University of Canterbury, Christchurch, New Zealand.

ABSTRACT

Pollen capture by kiwifruit flowers is a central problem in the kiwifruit industry, both by natural wind flow and by artificial air jet application. A commercial CFD code is used here to simulate the 3-dimensional air flow field around a single female kiwifruit flower at full bloom. The flow solutions from these models are compared in the air velocity range measured in kiwifruit orchards and at various flow-attacking angles. Particle transport models are then used in order to build a robust predictive model of pollen behaviour around a kiwifruit flower under a pollen-loaded air-jet.

NOMENCLATURE

A_f projected area of flower = 3.42×10^{-3} m^2
N_p number of pollen collected
Re Reynolds number
η_f pollen collection efficiency

INTRODUCTION

To produce an exportable 100-g kiwifruit (*Actinidia deliciosa*), between 6000 and 12000 viable male pollens need to be deposited on the stigma of a female kiwifruit flower (estimated from the data by Goodwin, 2000). Insufficient fertilization is known to lead to unsatisfactory fruit size, shape and uniformity, which represents a decreased marketable value. However, this pollination level must be completed in the limited six-day flowering period annually when the stigma are receptive (Gonzalez et al., 1995). This imposes serious constraints on the natural wind and bee pollinators which are often hampered by the wet weather, the delay in flowering between male and female flowers and the lack of attraction by flowers to bees. As a result, artificial pollination has become more popular because it offers great flexibility in timing and is used to supplement the inadequate pollination by wind and bee pollinators. Among different types of wet or dry spray-based machine application (see review by Goodwin, 2000), the dry air jet appears to be more promising due to its simplicity. The major cost of artificial pollination comes from the relatively expensive pure pollen supply and the labour. There is a need to optimise the pollen collection efficiency. We studied the air flow and pollen transport around a single kiwifruit flower using the commercial CFD code, CFX-5, with the pollen concentration at the background level in an orchard and at a more concentrated level as in an air jet application. The artificial pollination is usually applied when there is 30 to 40 % flower opening. Thus, in previous work (Hii et al., 2002), we looked at the air flow field around the buds at different opening stages, namely half-open, full-open and flip-back. Results of pollen capture only for a full-open female flower are presented here.

MODEL DESCRIPTION

Figure 1 shows one of the more than 200 female kiwifruit flowers photographed in Te Puke orchard area, New Zealand from 9-10 November 2001. This collection was studied to extract the detailed geometry for a model flower.

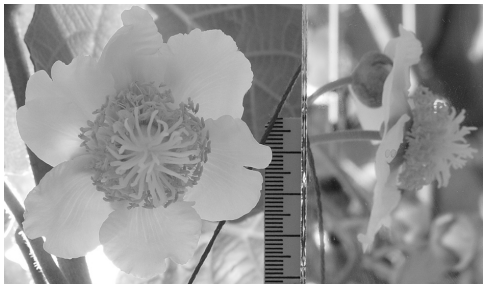

Figure 1: Front and side views of a full-open female kiwifruit flower (cv Hayward).

The flower model has an ovary, which is a truncated oblate spheroid 9.3 mm high, 9.0 mm diameter, and 3 and 7 mm diameter top and bottom (Figure 2).

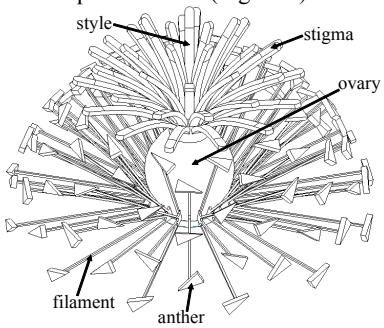

Figure 2: Flower model showing ovary, 36 stigma, 84 filaments and anthers. The filaments are 0.205 × 0.205 mm square rods, 14.2-15 mm long.

The ovary top has an expanding bush of 36 evenly spaced styles which are slightly curled but otherwise flat (0.9 mm in width, 0.5 mm in thickness and 9.5-10.5 mm in length). For economy of mesh, we did not fillet the edges of the style nor model it as a cylinder. Each style on an actual flower has a stigma at its tip (see Figure 3), which is the area of interest because only the pollen deposited here will germinate. A real stigma occupies about half of the style's circumferential surface. We define a pair of stigmatic surfaces at the tip of each style i.e. one on top and another on the bottom, to take into account that a real stigma can orient in any direction. Eighty four filaments, with a triangular anther (1.25 mm width × 2.7 mm high × 0.58 mm thick) at each end, extend from the base of the ovary and surround it. Although for ease of computation

the number of filaments is reduced from an average of 183 on a real flower (Hopping and Jerram, 1979), its density is visually comparable to that of an actual flower shown in Figure 1. The model flower has 6 petals, the average on most female flowers but some may have >7 petals. 3 pairs of overlapped 0.75-mm-thick petals (primary and secondary), with a gap along the overlap, are evenly spaced around the ovary in order to include the effect of flow leakage through the gap between the primary and secondary petals. The primary petal is constructed using the radial variation profile obtained by analysing a photo such as Figure 1. The secondary petal is then drawn to obtain a linear gap along the overlap up to a maximum gap of 5 mm. 6 sepals with their base and a 77-mm long stem (ϕ 2.73 mm) are placed under the petals. Any small gaps or isolated regions are eliminated manually for efficient meshing and better solver convergence.

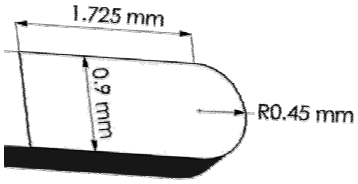

Figure 3: Shape of the model's planar stigmatic surface.

Simulation of wind pollination

We first studied the collection mechanism of windborne pollen by the flower under the average measured air velocity of 1 m/s (cf. maximum of 1.25 m/s recorded by Costa et al., 1993) from different directions, namely front, side and back. These simulate the wind pollination under the vine with the draft in random directions. The flower is treated as a bluff body in a computational domain shown in Figure 4 for a frontal flow (note that the air jet nozzle is not included in this wind simulation). The preliminary observations in a wind tunnel found that the petals of a 1-day-old flower remain rigid up to 1.8±0.1 m/s. The inlet and outlet boundaries (section 400 × 400 mm) are 200 mm and 350 mm away from the centre of the flower respectively. Other boundaries of the domain are of the "Opening" type with the Cartesian velocities set to be parallel to the inlet flow. The outlet boundary has a relative pressure of 0 Pa. The flower surfaces including the stigma are smooth with no slip.

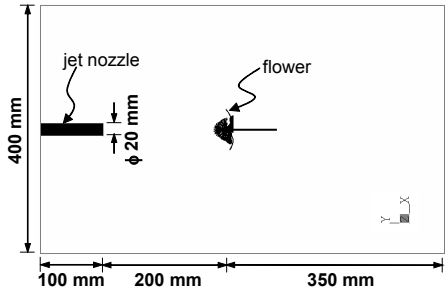

Figure 4: Schematic diagram of full-scale computational domain with an air jet nozzle in front of the flower.

The localized characteristic Re ranges from 50 to 4400 based on the dimension of style and the largest overall flower diameter (ϕ 66 mm). Since the localized flow varies from laminar coherent eddying to turbulent, we considered laminar, RNG k-ε (Yakhot et al., 1992) and SST (Menter, 1994) models. We found that all models gave a similar overall flow pattern but different magnitudes. RNG k-ε is chosen because its flow prediction is consistently between the other two models. It is applied with the built-in scalable wall treatment (Vieser et al., 2002). The incompressible air flow field is solved at steady state and isothermally at 25 ^{O}C, with a uniform inlet velocity and an assumed inlet turbulence intensity of 3.7 % in the absence of field data.

A maximum daily male pollen loading of 14.5 million grain/m^2/day in the orchard air has been reported by Malaboeuf et al. (1997), but the authors did not specify the average daily draft velocity. So, we decided to use our measured average velocity of 1 m/s in the orchard and this gives ~ 168 grain pollen/m^3 air. This means in our computational domain of 88×10^{-3} m^3, there are only ~ 15 pollen grains at any time and thus only the one-way fluid-particle coupling is considered. Since the injection of 15 pollen on the inlet boundary is not going to give a representative estimation of pollen collection efficiency from wind, 30000 pollens are injected uniformly on a ϕ 66-mm circular plane (with centre at the centre of the inlet boundary) which represents a projected area of the flower. The pollen passing through this circular plane may possibly collide and collect inertially on the flower. The pollen, having a solid density of 1330 kg/m^3 (Ferguson & Pusch, 1991) and an average diameter of 22 μm (Hopping, 1990; actual pollen are oblate spheroidal) are introduced at 1 m/s.

With the air as the continuous phase, the pollen (dispersed phase) trajectories are calculated in steady state using the Lagrangian framework (CFX-5.6 Manual, 2003; see the general equations in Ranade, 2002). The simulated pollen experience drag force and turbulent dispersion, but not gravitational force (the pollen settling velocity is low (~ 10 mm/s) compare to its superficial velocity of 1 m/s). The presence of papillar (Gonzalez et al., 1995) and liquid exudate (in the early morning) mean the pollen will stay on the stigma upon collision. Since it is unknown how the pollen will behave on the other surfaces of the flower, we assume that all the contacted pollen are captured. Other pollen leave the domain through the Opening and outlet boundaries.

Simulation of air jet sprayer

Following the results from the simulation of wind pollination, here we focus on introducing a pollen-loaded air jet onto the front of the flower (see domain setup in Figure 4). There are four initial air jet velocities - 0.5, 1.0, 2.0 and 3.0 m/s. The tubular flow is allowed to develop for 100 mm before being discharged from the ϕ 20-mm circular nozzle. The nozzle is located at the centre of the indicated domain boundary in Figure 4. All the side boundaries of the domain are assigned to be of the Opening type with a relative pressure of 0 Pa to handle the expanding air jet. The same turbulence model and wall treatment are applied to the air flow which is solved as in previous case, with all the walls regarded as smooth with no slip.

To find the pollen collection efficiency, the air jet releases 30000 non-coupled pollen which are tracked using the steady state Lagrangian approach. To estimate the effect of momentum coupling between the air and the pollen, we assume that 12000 pollen need to be collected by each flower at a collection efficiency of 5 % i.e. 240000 pollen

or 1.78-mg pollen/flower to be sprayed. A 1-second spray per flower gives a mass loading of 0.92-0.16 %wt in an air jet of 0.5-3.0 m/s. Despite this low mass loading, we still included the two-way coupling by employing a smaller set of pollen number (1000; using the recommendation in CFX-5.6 Manual, 2003) with a specified pollen mass flow rate of 1.78 mg/s. It has been found that this does not alter the air flow field. The particle-particle interaction is unlikely because the pollen volume fraction is 8.5×10^{-6} to 1.4×10^{-6} in this initial jet velocity range. All the walls, except for the jet nozzle, are assumed to be sticky to the pollen. The particle tracking also finishes at Opening boundaries.

Gridding

Figure 5 shows the gradual refinement of unstructured mesh closer to the flower surfaces. The number of elements is about 1 to 1.4 million with the maximum cell edge length ≤ 13 mm and the finest 0.1 mm. To promote better flow prediction in the region of interest, the styles and stigmas are covered with fine prismatic cells.

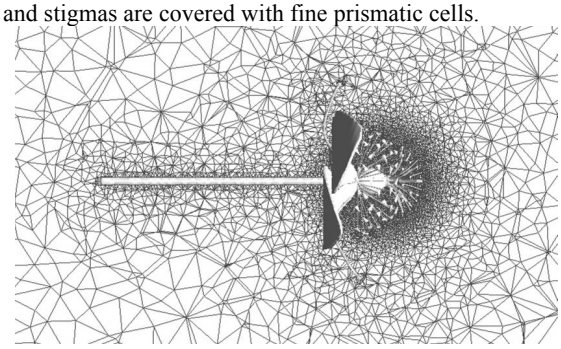

Figure 5: Generated mesh around a full-open flower.

RESULTS AND DISCUSSION

Collection of airborne pollen from wind

The streamline plots in Figure 6(a) to 6(c) for different approach directions show that the predicted flow fields are non-symmetrical and there are at least two recirculation regions, a larger recirculation downstream of the flower and some small eddies in the airspace between the stigma and the petals. The spiralling large wakes extend up to ~ 1.6 flower diameters downstream from the flower centre for the front and back flows. The pollen tracking calculations with side flow (Figure 6(e)) show that these large wakes help to redirect the pollen back to the stigmatic areas for secondary collection after the primary collection through the approaching flow. Under back flow, the role of the downstream wake becomes very important because all of the collected pollen on stigma rely on them. Figure 6(f) shows that most of the pollen follow the streamlines that are diverted to the sides by the petals. The large downstream vortices are found to incorporate these pollen grains and direct them straight to the stigma. This kind of backwards pollen collection has also been observed on other plants e.g. conifer ovulate cones (Niklas, 1984). However, this recirculated pollen collection is not important in front flow because of the impedance from the petals (Figure 6(d)). On the other hand, the eddies in the vicinity of the filament and stigma bushes have been found to trap the pollen. Although we expected that this will present more chances for trapped pollen to be deposited on the stigma, the simulations did not find any pollen collected in this way. This is because we assume that the filament and anther surfaces are sticky like the stigma. Thus the trapped pollen grains are filtered by the filament and anther surfaces before they reach the stigma.

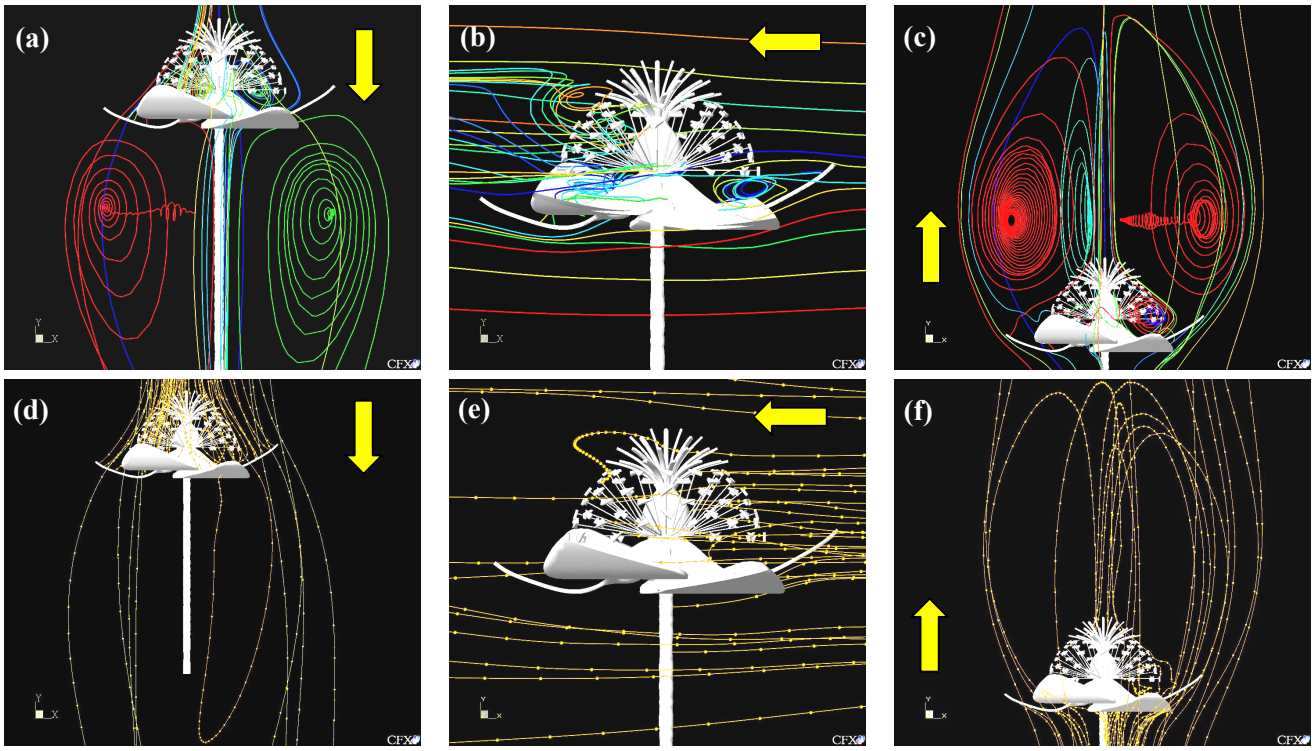

Figure 6: (a), (b) and (c) are the predicted air flow field around a single full-open flower under 1-m/s flow from the front, side and back respectively (as shown by the arrows). The corresponding calculated trajectories of a cloud of pollen are shown in (d), (e) and (f). The separation between pollen along a trajectory is 0.01 s.

The pollen collection efficiencies of stigma calculated based on the total number of pollen injected in different directions (through a circle the same diameter as the flower) are shown in Figure 7. It must be noted that these efficiencies have been halved because we defined a pair of stigmatic surfaces at the end of each style.

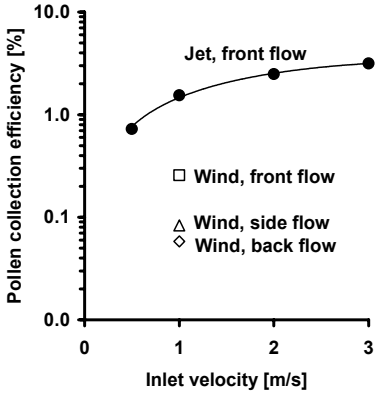

Figure 7: Calculated collection efficiency of windborne pollen and air-jet sprayed pollen by stigma of a full-open flower. The log scale is used for pollen collection efficiency.

According to Figure 7, the stigma capture the most pollen from a pollen cloud approaching in front flow (0.26 %), predominantly by direct impaction. The opposite is true for back flow. Due to our assumption of sticky surfaces, other surfaces of flower have been found to collect 10, 12 and 5 % of total pollen under front, side and back flows respectively, particularly on the petals. So, the actual pollen collection efficiency on the stigma may be higher than those shown in Figure 7 if the pollen rebound elastically on other flower surfaces.

Based on the efficiencies (η_f) in Figure 7, we estimate the number of windborne pollen collected by inertial impaction over 6 days under the maximum pollen loading reported by Malaboeuf et al. (1997) using Equation (1).

$$N_p = 14.5 \times 10^6 \text{ pollen/m}^2\text{/day} \times A_f \times \eta_f \times 6 \text{ days} \qquad (1)$$

A single female flower is expected to receive only 774, 238 and 179 windborne pollen grains in front, side and back flows respectively. This agrees with the experimental results from Costa et al. (1993) that wind pollination alone is insufficient.

We examined the number of pollen collected on each pair of stigma at the end of each style after 30000 pollen fed, and found that less than half of the 72 defined stigma have collected pollen (see Figure 8). No pollen is found to be deposited on the bottom face in each pair of stigma. If the bottom stigmatic face is regarded as leeward face, then all of the simulated pollens are deposited by direct interception on the forward faces (see particularly Figure 6(d) and (f)). The results with the bottom stigmatic surfaces may be different if the filaments and anthers are assumed to be non-sticky i.e. the small eddies within the flower enclosure can then deliver the pollen to the bottom stigmatic surfaces.

Although the draft in the vine is likely to have larger eddies than the flower itself, our simulated flow fields based on a uniform incoming flow are not expected to be significantly different to the actual ones. Since the simulation of wind pollination shows that pollen collection is favoured by the front flow, we now focus on spraying the concentrated pollen flow onto the front of a single female flower.

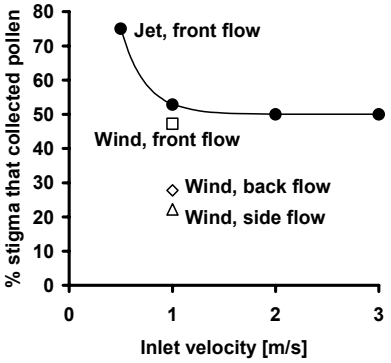

Figure 8: Percentage of 72 stigma that has windborne or sprayed pollen deposited on it, after 30000 were trialled in the simulation.

Collection of airborne pollen from air jet

With an air jet, the simulations show that the downstream eddies (see Figures 9(a) and 9(b)) are not as tidy and axisymmetrical as in the previous simulations with a uniform flow inlet where the downstream vortices have their centres along the ring of about the same diameter as the flower (see Figure 6(a)). This ring is ~ 0.54 flower diameters away from the flower centre. The pollen-loaded air jet also spreads more widely than is the case with uniform front flow after the impingement on the petals, likely due to the absence of surrounding flow. The comparison between Figure 9(a) and 9(b) shows that the degree of spread depends on the strength of jet.

Figure 10 is the profile of predicted centreline jet velocity from the discharge to the top of the ovary. The profile displays a slightly higher than initial jet velocity in the immediate discharge region. All four initial jet velocities then exhibit quite similar exponential decay although the lower initial jet velocity seems to have a faster decay. At around 160 mm away from the nozzle, there is a sudden drop of velocity due to the close distance approaching the ovary. This distance (~10 mm from the stigma) may be regarded as the stopping distance for the pollens to decelerate and be collected by the stigma. A plot of velocity profile across the stigma-style bush (Figure 11) shows that there is a stagnation region in the central bush. The velocity in the outer parts of the bush then increases up to ~ 60 % of the initial jet velocity before decreasing again, where the air flow sweeps past the stigma bush.

The jet Re number in this work ranges from 667 to 4000 based on the range of initial jet velocity used. So, strictly speaking the laminar model should be considered. However, we decided to select RNG k-ε based on the flower Re number. We compare the centreline velocity profile at initial jet velocity of 3 m/s with the turbulent free-jet formulae from Tuve (1953) and this is plotted between 140 and 160mm in Figure 10, the range where Tuve's formulae is valid. Our calculated velocity decay is under-estimated by 10.7 to 23.8 %. This may be because the RNG k-ε model has under-predicted the dissipation rate at this intermediate Re range here.

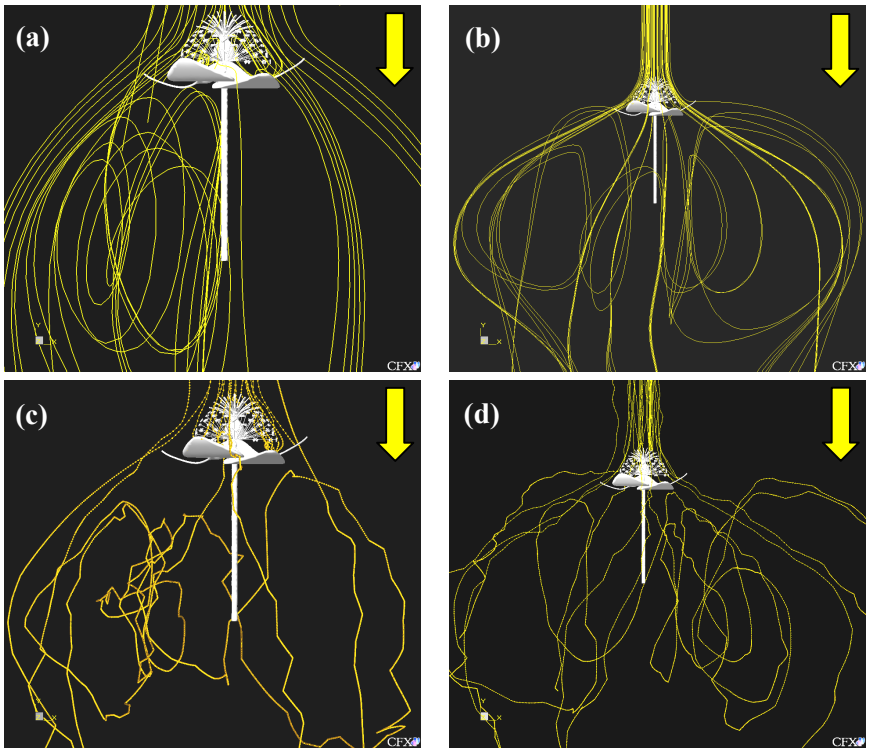

Figure 9: Simulations; (a) and (b) are the streamline plots from an air jet directed towards the front of the flower at 0.5 and 2.0 m/s respectively. The pollen movement around the flower under the respective jet velocities are shown in (c) and (d). The arrows indicate the direction of the air jet.

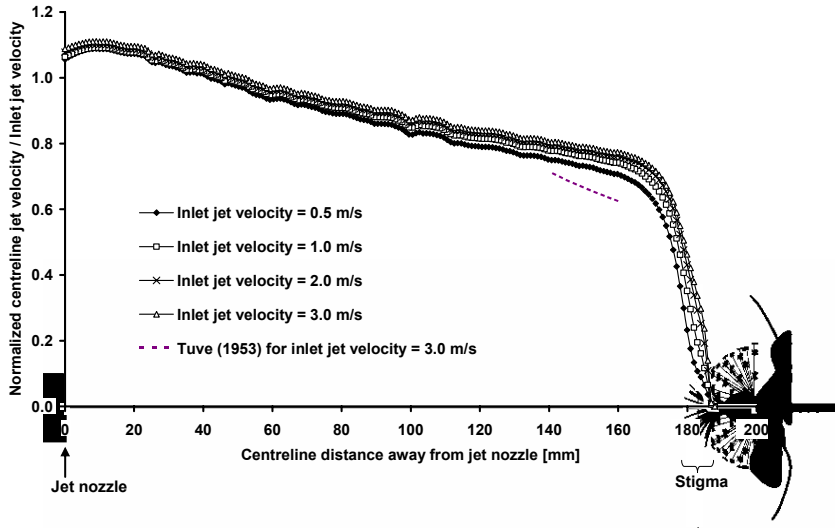

Figure 10: Jet centreline velocity.

The pollen trajectories under an air jet (Figure 9(c) and 9(d)) follow the overall pattern of streamlines to some degree but not the exact path. They appear to be more zigzagging, random and chaotic than those under the uniform velocity inlet (Figure 6(d)). There are a significant number of pollen grains trapped in the downstream vortices. But as mentioned before, the petals prevent any of this pollen from being re-collected by the stigma.

A higher velocity jet is found to give better collection efficiency as shown in Figure 7 (refer to values in Table 1). However, the gain in collection efficiency decreases with the increasing jet velocity. Considering the front flow in Figure 7, a possible reason why the flower collects more pollen in an air jet than in wind simulation is because in the latter case, the pollens are released over a larger projected area (ϕ 66 mm) compare to the nozzle diameter (ϕ 20 mm).

Based on the collection efficiencies in Figure 7 and the minimum required pollen capture of 6000 per flower, we estimate the minimum pollen loading of spray at different initial air jet velocities onto a single flower for one second (Table 1). Table 1 indicates that, for a circular ϕ 20-mm nozzle, by an increase of air jet from 0.5 m/s to 3.0 m/s will enable at least 3 more flowers to be sprayed for the equivalent amount of pollen.

Referring to Figure 8, it is found that only in air jets of 0.5 and 1.0 m/s have the bottom surface of each stigma pair at the end of each style been predicted to collect any pollen. This is indicated by the points with % stigma that collected pollen of more than 50 %. For an air jet at 0.5 m/s, about half of the bottom stigmatic faces are shown to have pollen deposited. It may be that at higher air jet velocity, the inertia of the pollen grains is too high to allow them to be collected by back-recirculation behind a single style. The effect of electrostatic in enhancing this type of collection is being studied.

Since the orientation of actual stigma is random, a lower air jet should be used, despite the lower collection efficiency, if a more consistent deposition over all the stigma is desired. Although the required total number of pollen for full fertilization does not have to be collected evenly by all the stigma (Howpage et al., 1995), it is known that the collection of too many pollen on a single flower can cause a lower number of seeds due to competition between pollen tube germinations (Hopping, 1990). From this perspective, there should be a compromise between the consistent pollen deposition and the collection efficiency in order to avoid local congestion on a stigma.

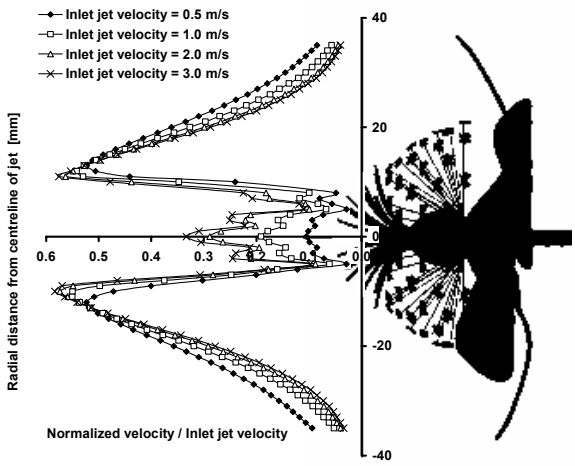

Figure 11: Velocity profile across the stigma bush.

In this flower model, the stigma are positioned at 2.3, 5.9, 8.6 and 10.6 mm along the horizontal stigma bush radius. The average number of pollen collected by each stigma generally increases towards the outer edge of the bush, but the maximum are predicted on stigma at either 5.9 or 8.6 mm.

Air jet velocity [m/s]	η [%]	Min. number of pollen per spray of one flower	Mass flow rate of pollen [mg/s]
0.5	0.73	8.2×10^5	6.1
1.0	1.54	3.9×10^5	2.9
2.0	2.48	2.4×10^5	1.8
3.0	3.17	1.9×10^5	1.4

Table 1: Minimum pollen loading required for capture of 6000 at different air jet velocities for a ϕ 20-mm circular nozzle.

Considering the practicality in placing a ϕ 20-mm jet nozzle accurately in front of a flower in the orchard, a larger nozzle size is expected to be exercised between this and the pollen injection area in wind simulation.

CONCLUSION

The simulations of wind pollination at the average draft velocity in an orchard show that a single female flower collects the most pollen in front flow compared to side and back flows. Large downstream recirculations are responsible for conveying the airborne pollen to the stigma in back flow. The depositions of pollen on stigma with uniform inlet velocity are from direct impaction only. On the other hand, the local eddies around each style are shown to assist the pollen collection at a low air jet velocity. This effect disappears at higher jet velocity as the bulk inertia from the incoming air jet dominates. The pollen collection increases with the increasing air jet velocity but with a gradual decrease in the gain in efficiency. An example of the pollen loading recommended for a ϕ 20-mm circular nozzle at different jet velocities has been provided.

ACKNOWLEDGEMENT

This work is funded by Zespri Innovation Company Limited, in their Postgraduate Fellowships scheme. We like to thank Peter Mulligan and Alistair Mowat, of Zespri for their advice and help. The support from David Fletcher and James Hart from ATD International was appreciated.

REFERENCES

CFX-5.6 Manual (2003), ANSYS.

COSTA, G., TESTOLIN, R. and VIZZOTO, G., (1993), "Kiwifruit pollination: an unbiased estimate of wind and bee contribution", *NZ J. of Crop and Hort. Sci.*, **21,** 189-195.

FERGUSON, A.M. and PUSCH, W.M., (1991), "Development of mechanical dry-pollen application to kiwifruit", *Acta Horticulturae 297*, ISHS, 299-304.

GONZALEZ, M.V., COQUE, M. and HERRERO, M., (1995), "Papillar integrity as an indicator of stigmatic receptivity in kiwifruit (*Actinidia deliciosa*)", *J. Exp. Bot.*, **46**, 263-269.

GOODWIN, R.M., (2000), *Zespri Innovation Kiwifruit Pollination Manual*, Zespri Innovation & The Hort. Research of New Zealand, New Zealand.

HII, M.J.W., ABRAHAMSON, J. and JORDAN, P.J., (2002), "CFD simulation of flow around a single kiwifruit flower", *5th Int. Symp. on Kiwifruit*, ISHS, Wuhan, China, September 15-20.

HOPPING, M.E., (1990), "Floral biology, pollination, and fruit set", In: WARRINGTON, I.J. and WESTON, G.C. (eds.), *Kiwifruit: Science and Management*, Ray Richards Publisher, Auckland, 71-96.

HOPPING, M.E. and JERRAM, E.M., (1979), "Pollination of kiwifruit (*Actinidia chinensis Planch.*): stigma-style structure and pollen tube growth", *NZ J. Botany*, **17**, 233-240.

HOWPAGE, D., VITHANAGE, V. and SPOONER-HART, R.N., (1998), "Pollen tube distribution in the Kiwifruit (*Actinidia deliciosa* A. Chev. C. F. Liang) pistil in relation to its reproductive process", *Annals of Botany*, **81**, 697-703.

MENTER, F.R., (1994), "Two-equation eddy-viscosity turbulence models for engineering applications", *AIAA J.*, **32,** 1598-1605.

MALABOEUF, F., VAISSIERE, B.E. and COUR, P., (1997), "Pollen flow in the atmosphere of kiwifruit (*Actinidia deliciosa*) orchards", In: SFAKIOTAKIS, E. and PORLINGIS, J. (eds.), *3rd Int. Symp. on Kiwifruit*, *Acta Horticulture*, 413-420.

NIKLAS, K.J., (1984), "The motion of windborne pollen grains around conifer ovulate cones: implications on wind pollination", *Amer. J. Bot.*, **71**, 356-374.

RANADE, V.V., (2002), *Computational Flow Modelling for Chemical Reactor Engineering*, Academic Press, San Diego, 85-122.

TUVE, G.L., (1953), "Air Velocities in Ventilating Jets", *Heat. Piping Air Cond.*, **25**, 181-191.

VIESER, W., ESCH, T. and MENTER, F., (2002), "Heat transfer predictions using advanced two-equation turbulence models", *AEA Technology validation report CFX-VAL10/0602*, Germany, www.software.aeat.com, 1-69.

YAKHOT, V., ORSZAG, S.A., THANGAM, S., GATSKI, T.B. and SPEZIALE, C.G., (1992), "Development of turbulence models for shear flows by a double expansion technique", *Physics of Fluids A: Fluid Dynamics*, **4,** 1510-1520.